Journal of Molecular Graphics and Modelling 34 (2012) 57–66

Contents lists available at SciVerse ScienceDirect

Journal of Molecular Graphics and Modelling

journal homepage: www.elsevier.com/locate/JMGM

Probing the effect of intermolecular interaction and understanding the electrostatic moments of anacardic acid in the active site of p300 enzyme via DFT and charge density analysis

B. Devipriya, P. Kumaradhas*

Laboratory of Biocrystallography and Computational Molecular Biology, Department of Physics, Periyar University, Salem 636 011, India

ARTICLE INFO

Article history:
Received 31 August 2011
Received in revised form
19 November 2011
Accepted 19 December 2011
Available online 27 December 2011

Keywords:
Anacardic acid
p300
Molecular docking
Intermolecular interaction
Dipole moment
Electrostatic potential

ABSTRACT

A charge density analysis has been performed on gas phase and docked forms of anacardic acid molecule to understand its charge density distribution, electrostatic moments and the conformation in the active site of p300 enzyme. Here, we report the binding affinity of anacardic acid with the p300 enzyme calculated from docking analysis. The charge density distribution of anacardic acid molecule in the gas phase as well as the docked form has been determined from the high level quantum chemical calculations using HF and DFT methods coupled with AIM theory. The charge density study on both forms of anacardic acid differentiates its structural and the electrostatic properties in different environments. When the molecule enters into the active site of p300 its conformation, charge density distribution, dipole moment and electrostatic potential are significantly altered in comparison to its gas phase structure. In the active site, the molecule adopts different conformations, its pentadecyl chain is found to be highly twisted; the charges are redistributed and the dipole moment increases from 2.37 to 3.17 D. Due to the charge redistribution, the electronegative region of carboxyl group increased as it is found small in the gas phase. The comparisons between both forms reveal the flexibility of anacardic acid in the active site.

1. Introduction

CREB binding protein (CBP) and p300 are homologous transcriptional coactivators [1] which contain several protein interaction domains including the histone acetyltransferase (HAT) domain. The function of p300/CBP mainly depends on these domains [2–4]. The main targets of the HATs in chromatin are N-terminal tails of the core histones, thus they acetylate the lysine residues of histones H2A, H2B, H3, and H4 [3]. During the acetylation, the p300 enzyme modulates the activity of transcription factors as well as the chromatin structure of their target genes [5]. The acetylation of proteins is a dynamic event involving in the enzymatic activities of histone acetyltransferases (HATs) and histone deacetylases (HDACs) [6]. Through their histone acetyltransferase activity these enzymes are involved in several biological processes like transcription, transformation, apoptosis, cell growth and division. The imbalanced HAT activity of p300/CBP has been implicated in several diseases [7–10] including cancer [11], asthma [12], diabetes [13], and cardiac hypertrophy [14]. Hence, the HAT activity of the p300 enzyme is being considered as the target for the generation of new therapeutics.

In the recent years, there are many HAT modulators (activators and inhibitors) are reported, but they are different from the histone deacetylases (HDACs). Some of the small molecules like anacardic acid (AA) [2-Hydroxy-6-pentadecyl-benzoic acid] [15], garcinol [6,16] and curcumin [17] were found as potent p300 or PCAF inhibitors. AA isolated from the cashew nut shell liquid (CNSL) is a first natural, nonspecific histone acetyltransferase inhibitor of p300 and p300/CBP associated factor (PCAF) [18]. Here, we have carried out the docking analysis to understand the binding affinity of ligand AA at the active site of p300. The binding of this ligand solely depends on the intermolecular interactions between the ligand and the amino acids present around the ligand at the active site. The intermolecular interaction alters the ligand structurally as well as electronically and these factors are also linked to its energetic nature at the active site . The main interest of this study is to explore the molecular conformation, charge density distribution and the electrostatic moments of the AA molecule before (gas phase) and after entering into the active site of p300.

Docking analysis gives the binding affinity and allows to understand the binding mode of the ligand in the active site of p300. Here, we have performed the docking study and carefully evaluated the nearest neighbours of the ligand AA, shortest intermolecular contacts between the ligand–p300, and the docked energies of AA molecule.

* Corresponding author. Tel.: +91 0 427 234552; fax: +91 0 427 2345565.
E-mail address: kumaradhas@yahoo.com (P. Kumaradhas).

1093-3263/$ – see front matter © 2012 Elsevier Inc. All rights reserved.
doi:10.1016/j.jmgm.2011.12.003

When the AA molecule enters into the active site of the p300, due to the intermolecular interactions between the AA–p300, the total energy and the geometry of the molecule changes and the molecule adopts a new conformation in the active site. The strength of ligand binding and its corresponding conformation plays a crucial role for the activation or inhibition of HAT activity in p300 enzyme. Further, the fine details of bond topological analysis and the electrostatic properties of AA in the active site gives the insight of binding affinity and the strength of intermolecular interactions. In order to understand the molecular flexibility in the active site and to precisely quantify the effect of intermolecular interactions in AA molecule a charge density analysis has been carried out in isolated form of AA (gas phase) from the quantum chemical calculations. Further, the charge density parameters of docked form of molecule (ligand lifted from the AA–p300 complex) have been compared with the gas phase structure. Eventually, we found a huge difference between the gas phase (I) and the docked (II) form of AA molecule; the exact differences have been discussed.

2. Computational details

Autodock [19] is a suite of program, used for flexible docking of ligand to protein. The complex form of three-dimensional structure of p300 HAT domain was obtained from Brookhaven Protein Data Bank (PDB code: 3BIY) [2]. For each docking, Autodock generated 10 different conformations and gave the value of corresponding docked energy. The ligand–protein complex and the intermolecular interactions between the protein and the ligand AA were viewed using PyMOL [20] software. Further, *ab initio* [21] and density functional calculations were performed to calculate the charge density distribution of (I) and (II) forms of AA using GAUSSIAN03 [22] program. The AA (I) has been optimized with 6-311G** basis set using Hartree–Fock (HF) [23] and DFT (B3LYP) [24,25] methods. A single point energy calculation has been carried out for the docked form of AA molecule (II) using the DFT method. The optimization of (I) was converged at threshold limits of 0.00045 and 0.0018 au for the maximum force and displacement, respectively. The bond topological properties such as the total electron density, the Laplacian of electron density, and bond ellipticity at the bond critical points (bcp) were determined from the Bader's theory [26] of atoms in molecules (AIM) using *ext94b* routine in AIMPAC [27] software. The deformation density of the molecule was plotted by *wfn2plots* and XD [28,29]. The electrostatic potential map has been plotted using Moliso [30] software.

3. Results and discussion

3.1. Molecular docking and anacardic acid–p300 interaction

We have carefully evaluated the results obtained from the docking analysis to understand the nearest neighbours of AA, the short contacts between AA and p300, and also its docked energies for the different conformational states. The ten lowest conformational energy state values are listed in Table 1. As of investigation, binding of this small molecule AA to the p300 enzyme leads to a structural change in the receptor p300 [16,31] and this structural change is responsible for the HAT inhibition [15,32]. Therefore, it is essential to know about the intermolecular interactions and the conformational geometry of AA to understand the molecular binding mechanism. Here, we have predicted some short contact interactions between the carbon atoms of AA and amino acid residues Trp1436 and Tyr1394 of receptor p300 (see Table 2); such type of interactions are also found in the reported experimental study on inhibitor Lys–CoA–p300 complex [2]. Hence, this evidence suggests that the shortest interactions are the prominent interactions, which are responsible for the HAT activity. AA contains carboxyl and hydroxyl groups; these groups are forming strong hydrophobic and hydrogen-bonding interactions with the p300 enzyme. Specifically, the oxygen atom of OH group makes a strong electrostatic interaction with the amino acid residue Arg1627 at a distance of 2.5 Å, whereas, the carbonyl oxygen forms a strong hydrogen bonding interaction with Tyr1397 at a distance of 1.82 Å (Fig. 1(a)). Further, the carbon atoms in the pentadecyl chain of AA forms some strong interactions with the oxygen atom of Ser1396. These interactions are also found in the docking analysis of CTPB and CTB with p300 [33]. Apart from these interactions, the molecule also forms strong electrostatic and van der Waals interactions with the other nearest neighbours of the active site (Table 2). Fig. 1(a) and (b) shows, some of the important strong interactions between AA and p300.

Table 1
The lowest docked energies (kcal/mol) of 10 different conformers of anacardic acid molecule.

Conformation	Lowest docked energy
1	−6.47
2	−6.45
3	−6.15
4	−5.27
5	−4.45
6	−4.29
7	−4.17
8	−2.98
9	−0.67
10	−0.33

3.2. Structural analysis

Fig. 2(a) and (b) shows the ball and stick model of (I) and (II) forms of AA molecule with the atom numbering scheme. Due to the weak and strong interactions between AA and p300, the conformation of AA has been modified and the molecule adopts a new conformation in the active site. The listed geometrical parameters of the two forms of AA in Table 3 show their exact conformational difference. On comparing (I) and (II), the pentadecyl chain of the docked form (II) has been twisted significantly (Fig. 2(a) and (b)) as it is linear in (I). This difference clearly shows that, when the molecule enters the active site of protein, the conformation of the ligand molecule changes, this is due to the strong intermolecular interaction between the AA and the amino acids of the active

Table 2
Nearest neighbours and short contact distance (Å) between anacardic acid and the atoms of amino acid residues of the active site of p300.

Anacardic acid atom···amino acid residue and identifier	Distance
C(6)···Gly1626/CA	3.10
O(1)···Arg 1627/HN	2.50
C(7)···Tyr1397/HH	2.76
O(2)···Tyr1397/HH	1.82
Tyr1397/OH	2.70
Tyr1397/CZ	3.05
C(9)···Glu1505/O	2.94
Gln1379/OE1	3.01
C(10)···Tyr1397/CE2	3.19
C(11)···Ser1396/O	2.93
Ser1396/CA	3.12
C(12)···Gly1506/O	2.94
Tyr1394/OH	3.13
Gly1506/C	3.17
C(13)···Tyr1394/OH	3.05
Gly1506/O	3.19
C(14)···Ser1396/O	2.57
C(15)···Trp1436/CE3	2.99
Tyr1394/HH	3.05
Tyr1394/OH	3.15
C(16)···Trp1436/O	3.14
C(17)···Ser1396/O	3.17

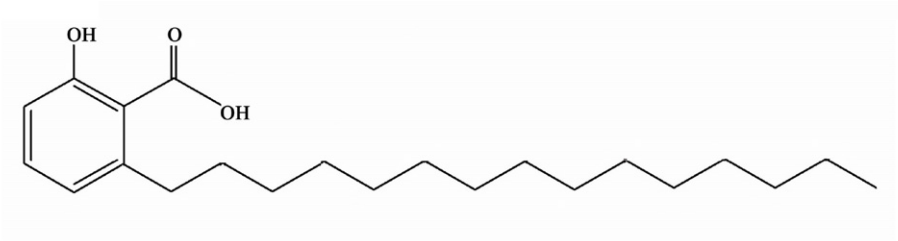

Anacardic acid

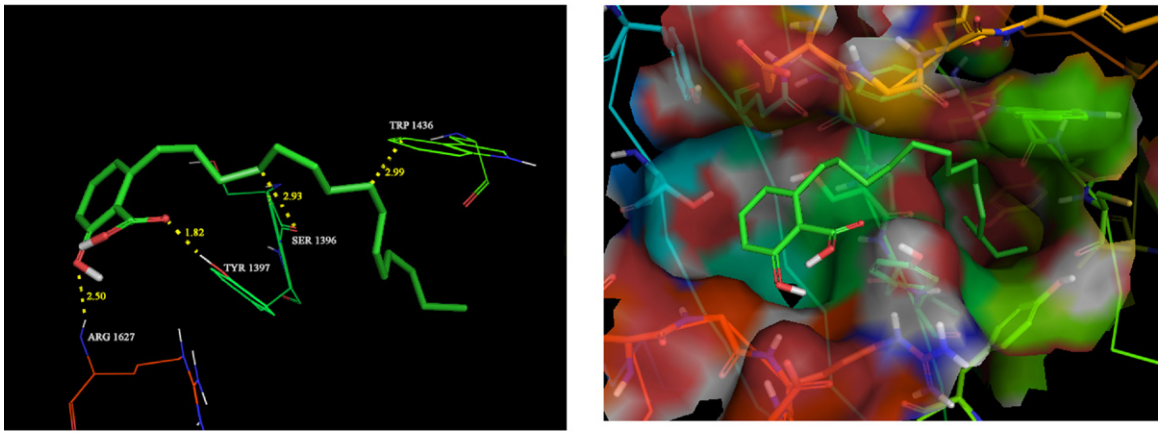

Fig. 1. (a) anacardic acid–p300 complex showing the intermolecular interactions and (b) Anacardic acid in the active site cavity of p300 enzyme.

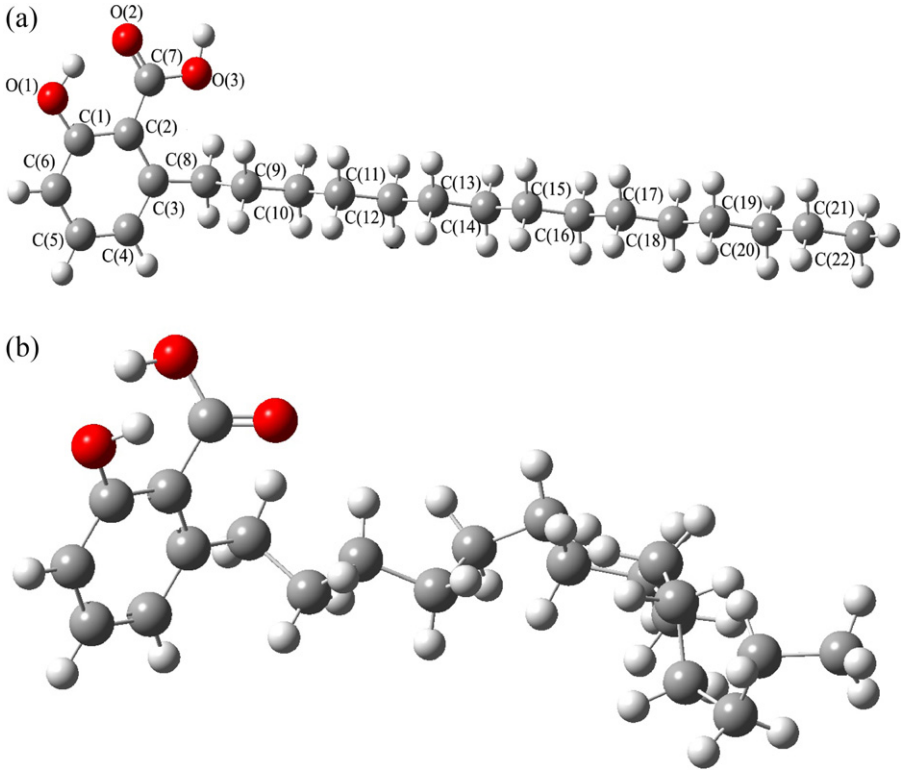

Fig. 2. (a) Optimized geometry of anacardic acid molecule (I) (gas phase) calculated from DFT/6-311G** with atomic numbering scheme and (b) geometry of the docked form of anacardic acid molecule (II).

Table 3
Geometrical parameters of two forms (I & II) of anacardic acid and the reported experimental values [13].

Bonds	I		II	Expr[b]
	HF	DFT	DFT (SP)[a]	
Bond lengths [Å]				
Aromatic ring				
C(1)—C(6)	1.394	1.400	1.421	1.397(5)
C(2)—C(1)	1.412	1.430	1.420	1.402(5)
C(2)—C(3)	1.423	1.428	1.421	1.422(5)
C(3)—C(4)	1.379	1.391	1.421	1.383(5)
C(4)—C(5)	1.391	1.397	1.420	1.368(5)
C(6)—C(5)	1.367	1.379	1.421	1.361(5)
OH group				
C(1)—O(1)	1.326	1.339	1.355	1.347(4)
COOH group				
C(2)—C(7)	1.480	1.471	1.516	1.468(5)
C(7)—O(2)	1.200	1.229	1.208	1.235(4)
C(7)—O(3)	1.321	1.348	1.338	1.314(4)
Pentadecyl chain				
C(3)—C(8)	1.521	1.518	1.496	1.510(5)
C(8)—C(9)	1.536	1.542	1.523	1.519(5)
C(9)—C(10)	1.529	1.532	1.523	1.513(5)
C(11)—C(10)	1.529	1.533	1.524	1.504(5)
C(11)—C(12)	1.529	1.533	1.524	1.504(5)
C(13)—C(12)	1.529	1.533	1.524	1.504(5)
C(14)—C(13)	1.529	1.533	1.522	1.500(5)
C(15)—C(14)	1.529	1.533	1.523	1.502(5)
C(15)—C(16)	1.529	1.533	1.523	1.498(5)
C(17)—C(16)	1.529	1.533	1.523	1.498(5)
C(17)—C(18)	1.529	1.533	1.523	1.508(5)
C(18)—C(19)	1.529	1.533	1.523	1.498(5)
C(19)—C(20)	1.529	1.533	1.523	1.507(5)
C(20)—C(21)	1.529	1.533	1.523	1.487(5)
C(21)—C(22)	1.528	1.531	1.523	1.475(5)
Bond angles [°]				
Aromatic ring				
C(1)—C(6)—C(5)	119.6	119.8	120.0	118.7(4)
C(2)—C(1)—C(6)	120.6	120.3	120.0	121.4(4)
C(2)—C(3)—C(4)	118.7	118.5	120.0	117.8(4)
C(3)—C(2)—C(1)	118.9	119.0	120.0	118.6(4)
C(3)—C(4)—C(5)	121.4	121.8	120.0	122.4(4)
C(6)—C(5)—C(4)	120.8	120.6	120.0	121.1(4)
COOH group				
C(1)—C(2)—C(7)	116.4	115.8	120.0	116.5(4)
C(3)—C(2)—C(7)	124.7	125.2	120.0	124.8(4)
O(2)—C(7)—C(2)	124.1	124.3	120.0	123.5(4)
O(2)—C(7)—O(3)	119.0	118.5	118.9	120.1(4)
O(3)—C(7)—C(2)	116.9	117.2	121.2	116.4(4)
OH group				
O(1)—C(1)—C(2)	124.2	123.4	120.0	124.0(4)
O(1)—C(1)—C(6)	115.2	116.2	120.0	114.6(4)
Pentadecyl chain				
C(2)—C(3)—C(8)	125.4	125.1	120.0	125.6(4)
C(3)—C(8)—C(9)	113.2	113.4	109.5	114.7(3)
C(4)—C(3)—C(8)	115.9	116.4	120.0	116.6(4)
C(8)—C(9)—C(10)	112.4	112.6	109.5	113.2(4)
C(10)—C(11)—C(12)	113.4	113.5	109.5	115.0(4)
C(11)—C(10)—C(9)	113.2	113.5	109.5	115.8(4)
C(11)—C(12)—C(13)	113.4	113.7	109.4	115.8(4)
C(14)—C(13)—C(12)	113.4	113.6	109.4	115.7(4)
C(14)—C(15)—C(16)	113.4	113.6	109.6	115.6(4)
C(15)—C(14)—C(13)	113.4	113.7	109.5	115.8(4)
C(15)—C(16)—C(17)	113.4	113.7	109.5	115.7(4)
C(17)—C(18)—C(19)	113.4	113.7	109.5	115.0(4)
C(18)—C(17)—C(16)	113.4	113.6	109.6	116.6(4)
C(18)—C(19)—C(20)	113.4	113.6	109.5	116.5(4)
C(19)—C(20)—C(21)	113.5	113.7	109.5	114.8(4)
C(20)—C(21)—C(22)	113.2	113.3	109.5	117.4(5)
Torsion angles [°]				
Aromatic ring				
C(1)—C(2)—C(3)—C(4)	−0.2	−0.3	0.1	0.0
C(1)—C(6)—C(5)—C(4)	0.0	0.0	0.0	0.0
C(2)—C(1)—C(6)—C(5)	−0.5	−0.5	0.0	−0.2
C(2)—C(3)—C(4)—C(5)	−0.3	−0.2	−0.1	−0.2
C(3)—C(2)—C(1)—C(6)	0.6	0.7	0.0	0.2
C(3)—C(4)—C(5)—C(6)	0.4	0.4	0.0	0.2
OH group				
C(3)—C(2)—C(1)—O(1)	−179.5	−179.3	179.4	179.8

Table 3 (*Continued*)

Bonds	I		II	Expr[b]
	HF	DFT	DFT (SP)[a]	
O(1)—C(1)—C(6)—C(5)	179.6	179.5	−179.5	−179.8
C(7)—C(2)—C(1)—O(1)	0.1	0.1	−1.2	−0.1
COOH group				
C(1)—C(2)—C(7)—O(2)	−1.8	−1.2	136.9	0.6
C(1)—C(2)—C(7)—O(3)	177.9	178.5	136.9	−178.7
C(3)—C(2)—C(7)—O(2)	177.8	178.2	−43.7	−179.3
C(3)—C(2)—C(7)—O(3)	−2.5	−2.1	135.9	1.4
C(7)—C(2)—C(1)—C(6)	−179.8	−179.9	179.4	−179.7
C(7)—C(2)—C(3)—C(4)	−179.8	−179.7	−179.4	179.9
C(7)—C(2)—C(3)—C(8)	1.3	1.6	0.0	1.3
Pentadecyl chain				
C(1)—C(2)—C(3)—C(8)	−179.1	−179.0	179.4	−178.6
C(2)—C(3)—C(8)—C(9)	83.9	83.4	117.3	79.7
C(3)—C(8)—C(9)—C(10)	−179.7	176.5	−88.2	172.8
C(4)—C(3)—C(8)—C(9)	−95.1	−95.3	−63.3	−98.9
C(8)—C(3)—C(4)—C(5)	178.7	178.6	−179.4	178.6
C(8)—C(9)—C(10)—C(11)	−178.7	178.0	−150.5	166.0
C(10)—C(11)—C(12)—C(13)	−180.0	178.0	156.5	157.3
C(12)—C(11)—C(10)—C(9)	−179.8	178.4	83.7	178.4
C(14)—C(13)—C(12)—C(11)	180.0	178.9	20.1	179.5
C(14)—C(15)—C(16)—C(17)	−180.0	179.4	−61.2	178.7
C(15)—C(14)—C(13)—C(12)	−180.0	178.9	138.0	177.4
C(16)—C(15)—C(14)—C(13)	180.0	179.4	−61.2	179.7
C(16)—C(17)—C(18)—C(19)	−180.0	179.7	−11.5	−179.1
C(17)—C(18)—C(19)—C(20)	−180.0	179.8	152.2	177.1
C(18)—C(17)—C(16)—C(15)	−180.0	179.7	−165.2	178.1
C(18)—C(19)—C(20)—C(21)	−180.0	179.9	0.4	−177.8
C(19)—C(20)—C(21)—C(22)	−180.0	179.7	−124.2	176.5

[a] SP-single point.
[b] Experiment.

site of p300 enzyme. This conformational modification can be well understood from the difference of torsion angles between (I) and (II) forms of AA and Fig. 2(a) and (b). The most affected groups in the molecule are the —COOH, —OH and the pentadecyl chain, which are predominantly involved in the intermolecular interactions. The C_{ar}—C_{ar} bond lengths of the aromatic ring of (I) and (II) vary from 1.379 to 1.430 Å and 1.420 to 1.421 Å respectively, in which the bond lengths of (II) are slightly shorter than (I). Specifically, the C(2)—C(1) [1.430 Å] and C(2)—C(3) [1.428 Å] bonds of (I) are found longer; whereas in (II), they are found shorter [C(2)—C(1): 1.420 and C(2)—C(3): 1.421 Å]; this bond shortening may be attributed to the presence of carboxyl group at the C(2) atom. In (II), the bond lengths of the C—C bonds of the pentadecyl chain are also found decreased. Owing to the conformational change of AA in the active site, the C—C—C bond angles of the pentadecyl chain are also decreased up to a maximum of ∼5°. As said earlier, the difference of torsion angles (Table 3) between both forms of AA reveals the exact conformational difference between the two forms. In (I), the C(3)—C(2)—C(7)—O(2) and C(3)—C(2)—C(7)—O(3) bonds exhibit *trans* and *cis* conformations and their corresponding torsion angles are 178.2 and −2.1° respectively. On the other hand, when the molecule enters into the active site (II), these conformations are changes to *gauche* and *trans* respectively and the corresponding torsion angles are −43.7 and 135.9°. Apart from these, a large conformational change also noticed in the pentadecyl chain of (II), this modification can be well understood from its torsion angles (Table 3). The geometrical parameters of both forms of AA molecule have been compared with the reported experimental parameters of AA [15].

3.3. Charge density analysis

The bond topological properties of the gas phase (I) and docked form (II) of the AA molecule are given in Table 4. The existence of (3, −1) type of bond critical point (bcp) in the bonds of the molecule, indicates the presence of chemical bonds between them. Fig. 3(a)–(d) displays the deformation density maps of the two forms of AA. This map shows the chemical bonding and the lone pair (non-bonding) positions of atoms in AA molecule. The deformation density map of pentadecyl chain of (II) is different from (I), this is due to the severe folding of chain in the active site. When the molecule enters into the active site of p300, subsequently its electron density is also redistributed due to the effect of intermolecular interactions. The electron density $\rho_{bcp}(r)$ in the C—C bonds of aromatic ring of (I) and (II) forms are ranges from 1.943 to 2.104 and 1.972 to 2.006 eÅ^{-3} respectively. These values are well agree with the reported aromatic ring [34]. On comparing the C—C bond densities of (I) and (II), the C_{ar}—C_{ar} bonds [∼1.986 eÅ^{-3}] of (II) are decreased, but the trend in the pentadecyl chain is opposite, where the C—C bond density [∼1.624 eÅ^{-3} in (I) and ∼1.662 eÅ^{-3} in (II)] has increased. These variations are largely attributed to the charge redistribution that occurs due to the effect of intermolecular interactions of the molecule in the active site. The $\rho_{bcp}(r)$ value of the carbonyl bonds at the COOH attachment varies significantly, in which the density of the C(7)—O(3) bond increases from 2.041 to 2.822 eÅ^{-3}, whereas in the C(7)═O(2) bond the value decreases from 2.695 to 2.082 eÅ^{-3}. In essence the large charge density difference between the two forms indicates that the charges are significantly migrated from one region of the molecule to the other region when the AA molecule present at the amino acid environment (active site of p300 enzyme). The electron density at the bcp of all bonds of (I) and (II) (Table 4) shows the exact differences. Fig. 4 illustrates, the difference of charge accumulation in —OH, —COOH groups and the pentadecyl chain of (I) and (II) forms.

The Laplacian of electron density [$\nabla^2\rho_{bcp}(r)$] bears the chemical significance of bond topological properties of the molecule. It provides the necessary information about the charge concentration/depletion at the bcp of the chemical bond [35,36]. The $\nabla^2\rho_{bcp}(r)$ value of C_{ar}—C_{ar} bonds of the two forms (I & II) range from −17.8 to −21.8, −18.2 to −18.8 eÅ^{-5} respectively, and these values are almost close with the reported values [37,38]. On

Table 4
Bond topological properties of the two forms (I & II) of anacardic acid molecule.

Bonds	$\rho_{bcp}(r)$[a]			$\nabla^2\rho_{bcp}(r)$[b]			ε		
	HF	DFT	DFT (SP)	HF	DFT	DFT (SP)	HF	DFT	DFT (SP)
Ring									
C(1)—C(2)	2.111	1.971	2.006	−23.1	−18.4	−18.8	0.302	0.236	0.262
C(2)—C(3)	2.035	1.943	1.972	−21.4	−17.8	−18.2	0.225	0.196	0.209
C(3)—C(4)	2.221	2.104	1.985	−25.1	−20.8	−18.5	0.277	0.230	0.201
C(4)—C(5)	2.173	2.078	1.982	−24.7	−20.8	−18.5	0.214	0.187	0.208
C(5)—C(6)	2.260	2.141	1.974	−26.2	−21.8	−18.4	0.266	0.219	0.206
C(6)—C(1)	2.199	2.096	1.996	−25.7	−21.2	−18.8	0.250	0.221	0.262
OH attachment									
C(1)—O(1)	2.111	2.065	1.949	−3.1	−10.4	−7.5	0.112	0.010	0.056
COOH attachment									
C(7)—C(2)	1.900	1.840	1.703	−20.2	−16.7	−14.3	0.186	0.178	0.098
C(7)—O(3)	2.139	2.041	2.822	−3.1	−12.1	−5.0	0.119	0.009	0.110
C(7)—O(2)	2.886	2.695	2.082	0.3	−8.0	−11.9	0.049	0.076	0.038
Chain attachment									
C(3)—C(8)	1.738	1.668	1.739	−17	−13.8	−15.0	0.022	0.027	0.031
C(8)—C(9)	1.684	1.581	1.639	−15.7	−12.2	−13.1	0.021	0.021	0.010
C(9)—C(10)	1.721	1.625	1.663	−16.4	−13.0	−13.5	0.016	0.016	0.006
C(10)—C(11)	1.719	1.623	1.659	−16.4	−12.9	−13.4	0.014	0.015	0.006
C(11)—C(12)	1.720	1.624	1.659	−16.4	−13.0	−13.4	0.014	0.015	0.011
C(12)—C(13)	1.720	1.624	1.652	−16.4	−13.0	−13.3	0.014	0.015	0.002
C(13)—C(14)	1.720	1.624	1.663	−16.4	−13.0	−13.5	0.014	0.015	0.003
C(14)—C(15)	1.720	1.624	1.660	−16.4	−13.0	−13.4	0.014	0.015	0.002
C(15)—C(16)	1.720	1.624	1.666	−16.4	−13.0	−13.5	0.014	0.015	0.003
C(16)—C(17)	1.720	1.624	1.661	−16.4	−13.0	−13.3	0.014	0.015	0.006
C(17)—C(18)	1.720	1.624	1.660	−16.4	−13.0	−13.5	0.014	0.015	0.005
C(18)—C(19)	1.720	1.624	1.660	−16.4	−13.0	−13.3	0.014	0.015	0.007
C(19)—C(20)	1.721	1.625	1.654	−16.4	−13.0	−13.3	0.014	0.015	0.002
C(20)—C(21)	1.722	1.626	1.658	−16.4	−13.0	−13.3	0.016	0.017	0.018
C(21)—C(22)	1.710	1.617	1.639	−16.3	−12.9	−13.2	0.008	0.008	0.012
C(4)—H(4)	1.974	1.899	1.958	−26.1	−23.1	−24.6	0.038	0.029	0.024
C(5)—H(5)	1.993	1.909	1.967	−26.9	−23.6	−25.0	0.003	0.009	0.013
C(6)—H(6)	1.980	1.903	1.954	−26.3	−23.3	−24.5	0.033	0.025	0.025
O(1)—H(1)	2.519	2.291	2.416	−69.8	−57.1	−58.5	0.017	0.017	0.025
O(3)—H(3)	2.585	2.427	2.415	−69.9	−60.4	−59.8	0.018	0.018	0.018
C(8)—H(8A)	1.982	1.897	1.994	−26.1	−22.9	−25.1	0.010	0.007	0.009
C(8)—H(8B)	1.942	1.864	1.943	−25.2	−22.1	−24.0	0.012	0.010	0.009
C(9)—H(9A)	1.940	1.868	1.955	−25.2	−22.2	−24.2	0.006	0.006	0.011
C(9)—H(9B)	1.922	1.852	1.955	−24.8	−21.9	−24.2	0.008	0.008	0.008
C(10)—H(10A)	1.909	1.841	1.975	−24.5	−21.6	−24.6	0.004	0.005	0.010
C(10)—H(10B)	1.912	1.843	1.949	−24.6	−21.6	−24.1	0.004	0.005	0.009
C(11)—H(11A)	1.911	1.843	1.996	−24.6	−21.6	−24.9	0.004	0.005	0.002
C(11)—H(11B)	1.912	1.843	1.939	−24.6	−21.6	−23.8	0.004	0.005	0.009
C(12)—H(12A)	1.910	1.841	1.952	−24.5	−21.6	−24.1	0.004	0.005	0.008
C(12)—H(12B)	1.911	1.842	1.951	−24.5	−21.6	−24.1	0.004	0.005	0.007
C(13)—H(13A)	1.911	1.842	1.954	−24.5	−21.6	−24.2	0.004	0.005	0.006
C(13)—H(13B)	1.911	1.842	1.952	−24.5	−21.6	−24.2	0.004	0.005	0.007
C(14)—H(14A)	1.910	1.841	1.984	−24.5	−21.6	−24.7	0.004	0.005	0.006
C(14)—H(14B)	1.910	1.842	1.958	−24.5	−21.6	−24.2	0.004	0.005	0.009
C(15)—H(15A)	1.910	1.842	1.943	−24.5	−21.6	−24.0	0.004	0.005	0.010
C(15)—H(15B)	1.911	1.841	1.946	−24.5	−21.6	−24.0	0.004	0.005	0.012
C(16)—H(16A)	1.910	1.841	1.973	−24.5	−21.6	−24.6	0.004	0.005	0.011
C(16)—H(16B)	1.910	1.842	1.948	−24.5	−21.6	−24.1	0.004	0.005	0.011
C(17)—H(17A)	1.910	1.842	1.960	−24.5	−21.6	−24.2	0.004	0.005	0.008
C(17)—H(17B)	1.910	1.841	1.945	−24.5	−21.6	−24.0	0.004	0.005	0.007
C(18)—H(18A)	1.910	1.841	1.948	−24.5	−21.6	−24.0	0.004	0.005	0.009
C(18)—H(18B)	1.910	1.842	1.989	−24.5	−21.6	−24.4	0.004	0.005	0.004
C(19)—H(19A)	1.910	1.842	1.995	−24.5	−21.6	−24.9	0.004	0.005	0.006
C(19)—H(19B)	1.910	1.841	1.945	−24.5	−21.6	−23.9	0.004	0.005	0.006
C(20)—H(20A)	1.910	1.841	1.955	−24.5	−21.6	−24.1	0.004	0.005	0.004
C(20)—H(20B)	1.910	1.841	1.950	−24.5	−21.6	−24.1	0.004	0.005	0.011
C(21)—H(21A)	1.916	1.847	2.018	−24.7	−21.8	−24.7	0.006	0.006	0.002
C(21)—H(21B)	1.916	1.847	1.939	−24.7	−21.8	−23.8	0.006	0.006	0.006
C(22)—H(22A)	1.906	1.841	1.930	−24.5	−21.6	−23.7	0.007	0.008	0.009
C(22)—H(22B)	1.910	1.845	1.934	−24.6	−21.8	−23.8	0.008	0.008	0.007
C(22)—H(22C)	1.906	1.841	1.939	−24.5	−21.7	−23.8	0.007	0.008	0.008

[a] In eÅ^{-3}.
[b] in eÅ^{-5}.

compare the $\nabla^2\rho_{bcp}(r)$ of C_{ar}—C_{ar} bonds of both forms, the are also concentrated in (II). Fig. 5 low negative values of Laplacian of (II) indicates the charges are depleted when AA present in the active site. Although a large conformational modification has taken place in the pentadecyl chain of (II), we have not noticed any substantial variation in $\nabla^2\rho_{bcp}(r)$ of C—C bonds of the chain. The C—O bonds in the docked form (II) of AA are highly depleted [C(1)—O(1): −7.5 and C(7)—O(3): −5.0 eÅ^{-5}] on compared with (I) [C(1)—O(1): −10.4 and C(7)—O(3): −12.1 eÅ^{-5}]. But in the C=O bond, the $\nabla^2\rho_{bcp}(r)$ of (II) [C(7)=O(2): −11.9 eÅ^{-5}] is concentrated than (I) [C(7)=O(2):

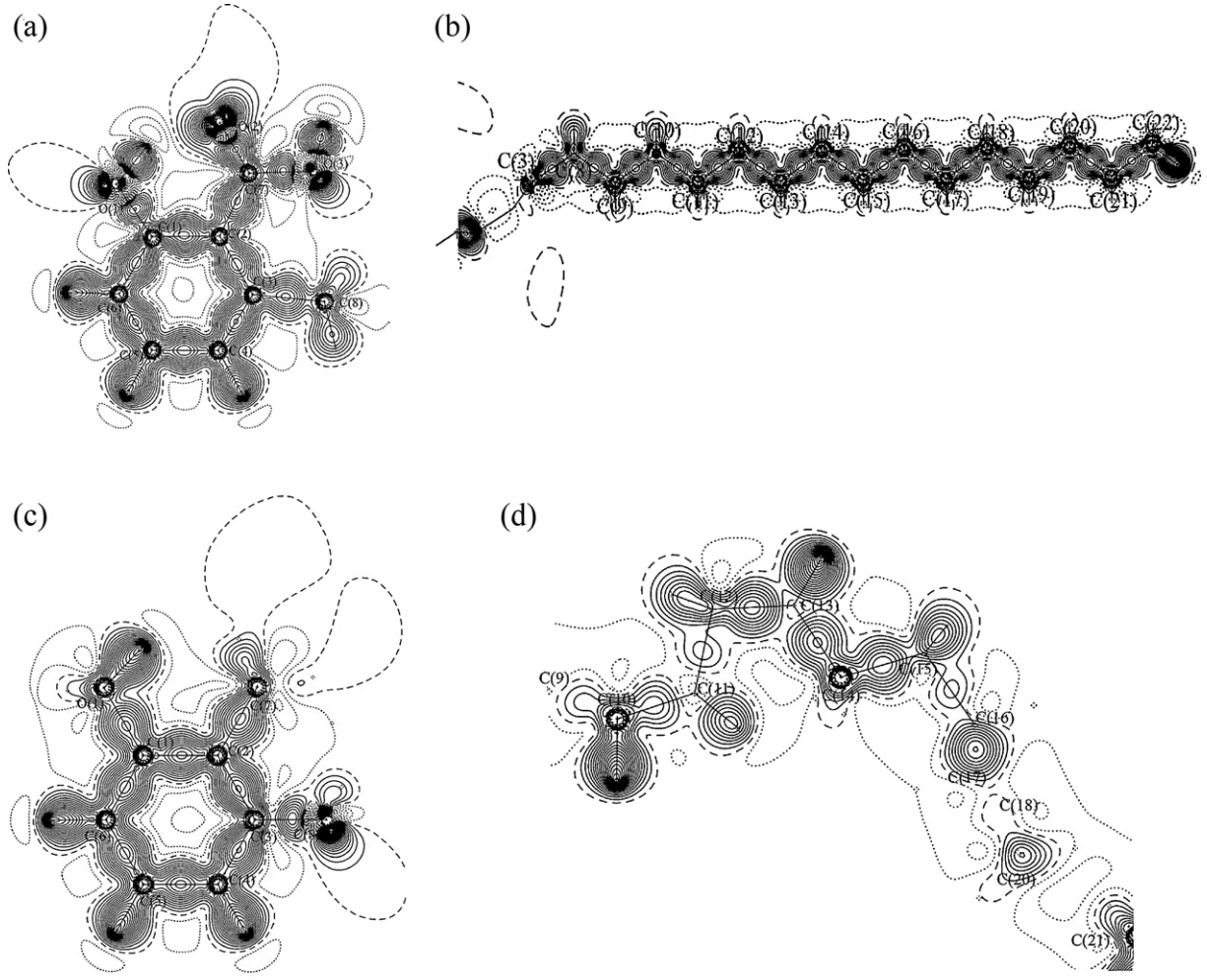

Fig. 3. Deformation density map of (a and b) (I) and (c and d) (II) forms of anacardic acid molecule. The positive (solid lines), negative (dotted lines) and zero contours (dashed line) are drawn at 0.05 eÅ^{-3} interval.

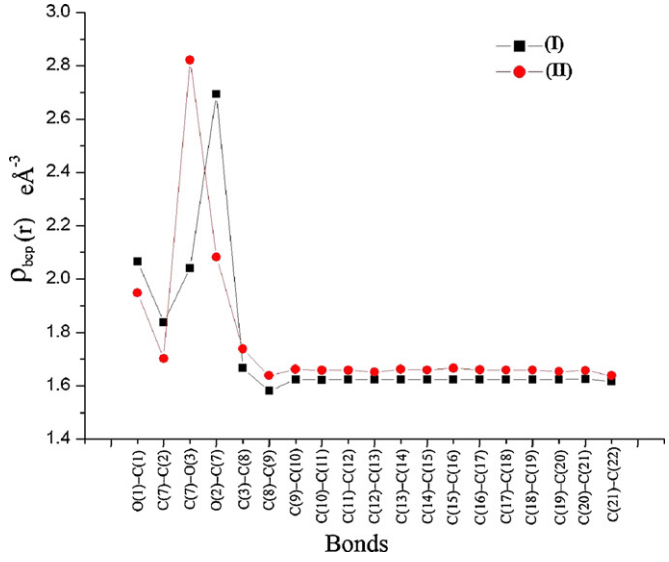

Fig. 4. Showing the difference between the deformation density of (I) and (II) forms of the OH, COOH and the pentadecyl chain of anacardic acid.

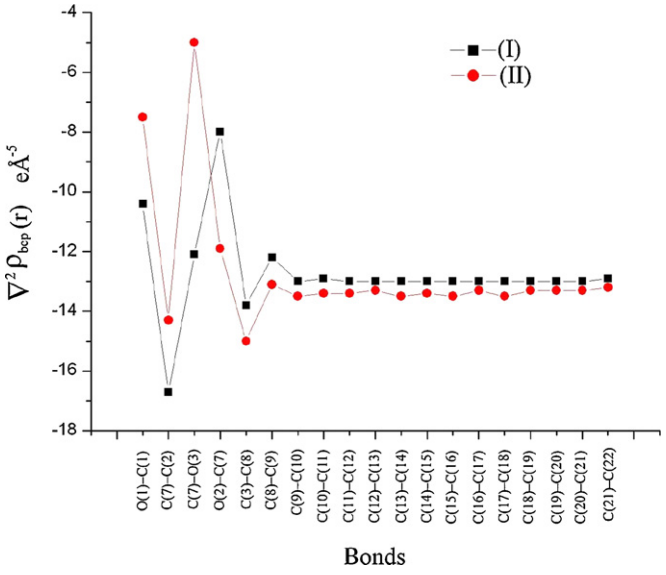

Fig. 5. Showing the difference of Laplacian of electron density of (I) and (II) forms of the OH, COOH and the pentadecyl chain of anacardic acid.

Table 5
Atomic charges (e) of two forms (I & II) of AA molecule (The first line for MPA and second line for NPA).

Atoms	I		II	Atoms	I		II
	HF	DFT	DFT (SP)		HF	DFT	DFT (SP)
C(1)	0.36	0.21	0.16	H(8B)	0.1	0.11	0.13
	0.5	0.41	0.34		0.17	0.19	0.2
C(2)	−0.36	−0.24	−0.13	H(9A)	0.1	0.11	0.12
	−0.35	−0.27	−0.24		0.17	0.19	0.19
C(3)	−0.04	−0.04	−0.05	H(9B)	0.09	0.11	0.11
	0.1	0.06	0.06		0.16	0.19	0.19
C(4)	−0.11	−0.07	−0.07	H(10A)	0.09	0.1	0.13
	−0.28	−0.25	−0.23		0.15	0.18	0.2
C(5)	−0.02	−0.06	−0.08	H(10B)	0.09	0.1	0.1
	−0.07	−0.14	−0.15		0.16	0.18	0.18
C(6)	−0.13	−0.08	−0.08	H(11A)	0.09	0.1	0.13
	−0.3	−0.27	−0.26		0.16	0.18	0.2
C(7)	0.7	0.47	0.3	H(11B)	0.09	0.1	0.11
	0.99	0.82	0.8		0.16	0.18	0.19
C(8)	−0.16	−0.2	−0.2	H(12A)	0.09	0.1	0.11
	−0.34	−0.4	−0.41		0.15	0.18	0.19
C(9)	−0.14	−0.17	−0.22	H(12B)	0.09	0.1	0.11
	−0.3	−0.36	−0.36		0.16	0.18	0.18
C(10)	−0.19	−0.21	−0.2	H(13A)	0.09	0.1	0.12
	−0.31	−0.37	−0.36		0.15	0.18	0.19
C(11)	−0.18	−0.2	−0.25	H(13B)	0.09	0.1	0.11
	−0.31	−0.36	−0.38		0.16	0.18	0.19
C(12)	−0.18	−0.2	−0.22	H(14A)	0.09	0.1	0.13
	−0.31	−0.36	−0.38		0.15	0.18	0.19
C(13)	−0.18	−0.2	−0.17	H(14B)	0.09	0.1	0.12
	−0.31	−0.36	−0.36		0.15	0.18	0.19
C(14)	−0.18	−0.2	−0.29	H(15A)	0.09	0.1	0.1
	−0.31	−0.36	−0.4		0.15	0.18	0.18
C(15)	−0.18	−0.2	−0.18	H(15B)	0.09	0.1	0.1
	−0.31	−0.36	−0.35		0.16	0.18	0.18
C(16)	−0.18	−0.2	−0.29	H(16A)	0.09	0.1	0.11
	−0.31	−0.36	−0.38		0.15	0.18	0.19
C(17)	−0.18	−0.2	−0.17	H(16B)	0.09	0.1	0.1
	−0.31	−0.36	−0.37		0.15	0.18	0.18
C(18)	−0.17	−0.2	−0.23	H(17A)	0.09	0.1	0.12
	−0.31	−0.36	−0.34		0.15	0.18	0.18
C(19)	−0.17	−0.2	−0.24	H(17B)	0.09	0.1	0.11
	−0.31	−0.37	−0.38		0.15	0.18	0.19
C(20)	−0.18	−0.2	−0.21	H(18A)	0.09	0.1	0.12
	−0.31	−0.37	−0.37		0.15	0.18	0.2
C(21)	−0.2	−0.22	−0.27	H(18B)	0.09	0.1	0.11
	−0.31	−0.36	−0.36		0.15	0.18	0.16
C(22)	−0.23	−0.29	−0.28	H(19A)	0.09	0.1	0.15
	−0.49	−0.56	−0.56		0.15	0.18	0.2
O(1)	−0.45	−0.35	−0.38	H(19B)	0.09	0.1	0.11
	−0.73	−0.66	−0.7		0.15	0.18	0.19
O(2)	−0.54	−0.42	−0.31	H(20A)	0.09	0.1	0.1
	−0.75	−0.66	−0.58		0.15	0.18	0.18
O(3)	−0.42	−0.33	−0.27	H(20B)	0.09	0.1	0.11
	−0.74	−0.68	−0.66		0.15	0.18	0.19
H(1)	0.3	0.27	0.26	H(21A)	0.09	0.1	0.13
	0.51	0.49	0.21		0.16	0.18	0.17
H(3)	0.28	0.26	0.24	H(21B)	0.09	0.1	0.11
	0.49	0.48	0.47		0.16	0.18	0.19
H(4)	0.09	0.08	0.1	H(22A)	0.08	0.1	0.09
	0.19	0.2	0.47		0.16	0.19	0.18
H(5)	0.1	0.1	0.11	H(22B)	0.09	0.11	0.1
	0.19	0.2	0.2		0.17	0.19	0.19
H(6)	0.11	0.11	0.11	H(22C)	0.08	0.1	0.09
	0.21	0.22	0.21		0.16	0.19	0.18
H(8A)	0.13	0.13	0.14				
	0.19	0.22	0.23				

$-8.0\,e\text{Å}^{-5}$]. Similarly, the C—H bonds, shows the difference of Laplacian of electron density between (I) and (II) forms of OH and COOH groups and the pentadecyl chain.

Bond ellipticity (ε) is being used to understand the spherical/aspherical nature of the bond electron density [39]. It is the evaluation of the degree of planarity or conjugation of the bond density. Ellipticity can be calculated from $\varepsilon = (\lambda_1/\lambda_2) - 1$, where, λ_1 and λ_2 are the Hessian eigen values of the density at the bond critical points. If the value of ε is maximum it indicates the double bond character and zero indicates the triple bond character of the bond. In the present study, in both forms, the ε of C—C bonds of the aromatic ring are found large and the value is ~0.2, which is greater than the C—C bonds in the chain (Table 4) and these values are well agree with the reported experimental values [40]. The large values of ε confirms that electron density distribution of C_{ar}—C_{ar} bonds of both forms are anisotrophic.

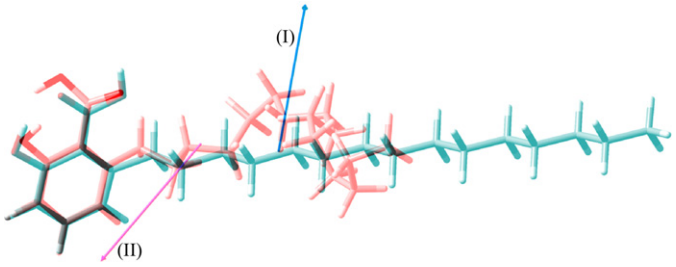

Fig. 6. Molecular dipole moment of (I) [blue] and (II) [red] forms of anacardic acid. The origin is at the centre of the mass of the molecule. (For interpretation of the references to color in this figure legend, the reader is referred to the web version of the article.)

3.4. Electrostatic moments

When the molecule enters into the active site of p300 enzyme, the atomic charges of the molecule are also significantly altered. This can be well understood from the difference of atomic charges between the (I) and (II). The atomic charges of both forms were calculated from the Mulliken population analysis (MPA) [41] and Natural population analysis (NPA) [42] (Table 5). On comparing the docked form with the gas phase molecule, the charges of the C(1) [0.16 e] and C(2) [0.13 e] atoms are found to be less, this difference may be attributed to the participation of hydrogen bonding interactions of OH and COOH groups, which are attached with C(1) and C(2) atoms respectively. The charges of both O(2) [−0.31 e] and O(3) [−0.27 e] atoms are also decreased. The atomic charges in the pentadecyl chain are also redistributed (Table 5). Notably, in both forms of AA molecule, the hydrogen atoms carry almost equal amount of positive charges [∼0.11 e].

The dipole moment (μ) of the molecule results from the atomic charge distribution in the molecule. The molecular dipole moment of (I) and the docked (II) forms of AA molecule has been calculated from HF and DFT methods. The predicted dipole moment of the gas phase (I) is 2.37 D, which is found much smaller than the docked form (II) [3.17 D] and the difference is ∼1 D. This indicates that, when the AA molecule enters into the active site of the p300 enzyme the net dipole moment of the molecule increased and the orientation of the dipole moment vector also changed (Fig. 6). This dipole moment enhancement is due to the charge redistribution and migration of charges from one region of molecule to the other region caused by the intermolecular interactions between the ligand and p300 enzyme [43]. Fig. 6 shows the superimposed forms of (I) and (II) and the orientation of the dipole moment vectors of AA in the active site of p300 (Table 6).

Table 6
Magnitude of molecular dipole moment (Debye) of two forms (I & II) of anacardic acid calculated from HF and DFT methods.

Forms	Method	μ_x	μ_y	μ_z	μ
(I)	HF	−2.232	−1.093	1.038	2.693
(I)	DFT	−2.030	−0.818	0.916	2.372
(II)	DFT (SP)	−1.808	−1.803	−1.875	3.168

The electrostatic potential (ESP) of molecule is mainly used to investigate the intermolecular interactions between the ligand–receptor [44]. Fig. 7(a) and (b) shows the isosurface representation of the molecular electrostatic potential (MEP) of (I) and (II) forms. The negative (red) and positive (blue) regions of the MEP were plotted for the +0.25 and −0.019 au isosurface values. Fig. 7(a) displays a very small amount of negative potential at the vicinity of O(2) and O(3) atoms of the carboxyl group; on the other hand, the O(1) atom of the hydroxyl group possesses more positive potential. But in (II) (Fig. 7(b)), a large electronegative region of ESP is found at the vicinity of O(2) and O(3) atoms; this enhancement is solely attributed to the extended charge accumulation in the polar groups due to the interaction of molecule with the neighbouring amino acids present at the active site of p300 and the charge redistribution.

4. Conclusion

The docking and theoretical charge density studies on anacardic acid molecule differentiate its conformational, bond topological and the electrostatic properties from its gas phase form. When the molecule present in the active site of p300, due to the intermolecular interaction between anacardic acid and p300, the charges are redistributed and the conformation of the molecule also changed. Anacardic acid forms electrostatic interaction with the amino acid residues Arg1627, Ser1396, and Trp1436; specifically, it forms strong hydrogen bonding interaction with Tyr1397 at the distance 1.82 Å. The bond topological properties of both the forms of the molecule differentiate the exact difference of charge distribution between the two forms. The dipole moment of the isolated form is 2.37 D, when the molecule enters into the active site of p300, the dipole moment increases to 3.17 D. This dipole moment enhancement may be attributed to the intermolecular interactions between the anacardic acid molecule and the p300 enzyme. The molecular electrostatic potential is not same in both forms, a significant difference has been noticed, specifically, the

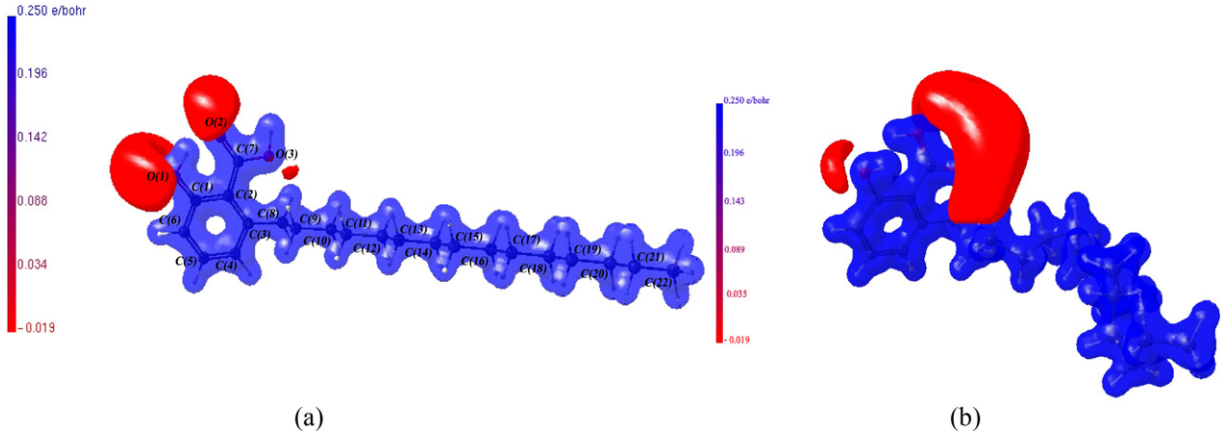

Fig. 7. Isosurface representation of molecular electrostatic potential of anacardic acid in (a) gas phase (I) and (b) at the active site of p300 enzyme (II). Blue: positive potential (+0.28 eÅ^{-1}), red: negative potential (−0.02 eÅ^{-1}). (For interpretation of the references to color in this figure legend, the reader is referred to the web version of the article.)

negative ESP near the carboxyl group is found increased, whereas in the hydroxyl group this has been decreased.

References

[1] Z. Arany, L.E. Huang, R. Eckner, S. Bhattacharya, C. Jiang, M.A. Goldberg, H.F. Bunn, D.M. Livingston, An essential role for p300/CBP in the cellular response to hypoxia, Proc. Natl. Acad. Sci. U.S.A. 93 (1996) 12969–12973.

[2] X. Liu, L. Wang, K. Zhao, P.R. Thompson, Y. Hwang, R. Marmorstein, P.A. Cole, The structural basis of protein acetylation by the p300/CBP transcriptional coactivator, Nature 451 (2008) 846–850.

[3] E. Kalkhoven, CBP and p300: HATs for different occasions, Biochem. Pharmacol. 68 (2004) 1145–1155.

[4] L.W. Yuan, A. Giordano, Acetyltransferase machinery conserved in p300/CBP-family proteins, Oncogene 21 (2002) 2253–2260.

[5] N. Forster, S. Gallinat, J. Jablonska, S. Weiss, H.P. Elsasser, W. Lutz, p300 protein acetyltranferase activity suppresses systemic lupus erythematosus-like autoimmune disease in mice, J. Immunol. 178 (2007) 6941–6948.

[6] G. Sbardella, S. Castellano, C. Vicidomini, D. Rotili, A. Nebbioso, M. Miceli, L. Altuccic, A. Mai, Identification of long chain alkylidenemalonates as novel small molecule modulators of histone acetyltransferases, Bioorg. Med. Chem. Lett. 18 (2008) 2788–2792.

[7] L. Wei, N. Jamonnak, J. Choy, Z. Wang, W. Zheng, Differential binding modes of the bromodomains of CREB-binding protein (CBP) and p300 with acetylated MyoD, Biochem. Biophys. Res. Commun. 368 (2008) 279–284.

[8] K. Mantelingu, B.A. AshokReddy, V. Swaminathan, A. Hari Kishore, N.B. Siddappa, G.V. Pavan Kumar, G. Nagashankar, N. Natesh, S. Roy, P.P. Sadhale, U. Ranga, C. Narayana, T.K. Kundu, Specific inhibition of p300-HAT alters global gene expression and represses HIV replication, Chem. Biol. 14 (2007) 645–657.

[9] F.D. Piaz, A. Vassallo, O.C. Rubio, S. Castellano, G. Sbardella, N.De. Tommasi, Chemical biology of histone acetyltransferase natural compounds modulators, Mol. Divers. 15 (2011) 401–416.

[10] M.W. Rekowski, A. Giannis, Histone acetylation modulation by small molecules: a chemical approach, Biochim. Biophys. Acta 1799 (2010) 760–767.

[11] Y. Ionov, S.I. Matsui, J.K. Cowell, A role for p300/CREB binding protein genes in promoting cancer progression in colon cancer cell lines with microsatellite instability, Proc. Natl. Acad. Sci. U.S.A. 101 (2004) 1273–1278.

[12] K. Ito, C.E. Charron, I.M. Adlock, Impact of protein acetylation in inflammatory lung diseases, Pharmacol. Ther. 116 (2007) 249–265.

[13] S.G. Gray, D.P. Meyts, Role of histone and transcription factor acetylation in *diabetes* pathogenesis, Diabetes Metab. Res. Rev. 21 (2005) 416–433.

[14] T. Kakita, K. Hasegawa, T. Morimoto, S. Kaburagi, H. Wada, S. Sasayama, p300 protein as a coactivator of GATA-5 in the transcription of cardiac-restricted atrial natriuretic factor gene, J. Biol. Chem. 274 (1999) 34096–34102.

[15] K. Balasubramanyam, V. Swaminathan, R. Anupama, T.K. Kundu, Small molecule modulators of histone acetyltransferase p300, J. Biol. Chem. 278 (2003) 19134–19140.

[16] M. Arif, S.K. Pradhan, G.R. Thanuja, B.M. Vedamurthy, S. Agrawal, D. Dasgupta, T.K. Kundu, Mechanism of p300 specific histone acetyltransferase inhibition by small molecules, J. Med. Chem. 52 (2009) 267–277.

[17] S.B. Kutluay, J. Doroghazi, M.E. Roemer, S.J. Triezenberg, Curcumin inhibits herpes simplex virus immediate-early gene expression by a mechanism independent of p300/CBP histone acetyltransferase activity, Virology 373 (2008) 239–247.

[18] I. Kubo, M. Ochi, P.C. Vieira, S. Komatsu, Antitumor agents from the cashew (Anacardium occidentale) apple juice, J. Agric. Food. Chem. 41 (1993) 1012–1015.

[19] G.M. Morris, R.S. Goodsell, R.S. Halliday, R. Huey, W.E. Hart, R.K. Belew, A.J. Olson, Automated docking using a lamarckian genetic algorithm and empirical binding free energy function, J. Comput. Chem. 19 (1998) 1639–1662.

[20] W.L. DeLano, PyMol Molecular Graphics System, DeLano Scientific, San Carlos, CA, USA, 2002.

[21] S.J. Smith, B.T. Sutcliffe, The development of computational chemistry in the United Kingdom, Rev. Comput. Chem. 10 (1997) 271–316.

[22] M.J. Frisch, G.W. Trucks, H.B. Schlegel, G.E. Scuseria, M.A. Robb, J.R. Cheeseman, J.A. Montgomery Jr., Vreven, K.N. Kudin, J.C. Burant, J.M. Millam, S.S. Iyengar, J. Tomasi, V. Barone, B. Mennucci, M. Cossi, G. Scalmani, N. Rega, G.A. Petersson, H. Nakatsuji, M. Hada, M.P. Ehara, K. Toyota, R. Fukuda, J. Hasegawa, M. Ishida, T. Nakajima, Y. Honda, O. Kitao, H. Nakai, M. Klene, X. Li, J.E. Knox, H.P. Hratchian, J.B. Cross, Adamo, J. Jaramillo, R. Gomperts, R.E. Stratmann, O. Yazyev, A.J. Austin, R. Cammi, C. Pomelli, J.W. Ochterski, P.Y. Ayala, Morokuma, G.A. Voth, P. Salvador, J.J. Dannenberg, V.G. Zakrzewski, S. Dapprich, A.D. Daniels, M.C. Strain, O. Farkas, D.K. Malick, A.D. Rabuck, K. Raghavachari, J.B. Foresman, J.V. Ortiz, Q. Cui, A.G. Baboul, S. Clifford, J. Cioslowski, B.B. Stefanov, G. Liu, A. Liashenko, P. Piskorz, I. Komaromi, R.L. Martin, D.J. Fox, T. Keith, M.A. Al-Laham, C.Y. Peng, A. Nanayakkara, M. Challacombe, P.M.W. Gill, B. Johnson, W. Chen, M.W. Wong, C. Gonzalez, J.A. Pople, Gaussian 03, Revision D.1, Gaussian, Inc., Wallingford, CT, 2005.

[23] A.R. Leech, Molecular Modelling Principles and Applications, Addison Wesley Longman, Essex, England, 1996.

[24] J.K. Labanowski, J.W. Andzelm, Density Functional Methods in Chemistry, Springer, New York, 1991.

[25] R.G. Parr, W. Yang, Density Functional Theory of Atoms and Molecules, Oxford, New York, 1989.

[26] R.F.W.Bader, Y. Tal, S.G. Anderson, T.T. Nguyen-Dang, Isr. J. Chem. 19 (1980) 8–29.

[27] J. Cheeseman, T.A. Keith, R.F.W. Bader, AIMPAC Program Package, McMaster University, Hamilton, Ontario, 1992.

[28] T. Koritsanszky, P. Macchi, C. Gatti, L.J. Farrugia, P.R. Mallinson, A. Volkov, T. Richter, XD-2006. A Computer Program Package for Multipole Refinement and Topological Analysis of Charge Densities and Evaluation of Intermolecular Energies from Experimental or Theoretical Structure. Factors, Version 5.33, 2007.

[29] T. Koritsanszky, T. Richter, P. Macci, C. Gatti, S. Howard, P.R. Mallinson, L.J. Farrugia, Z.W. Su, N.K. Hansen, X.D. – A Computer Program Package for Multipole Refinement and Analysis of Electron Densities from Diffraction Data, Freie Universitï, Berlin, 2003.

[30] C.B. Hubschle, P. Luger, Moliso – a program for colour-mapped iso-surfaces, J. Appl. Crystallogr. 39 (2006) 901–904.

[31] K. Mantlingu, A. HariKishore, K. Balasubramanyam, G.V. PavanKumar, M. Altaf, S. Nanjunda Swamy, R. Selvi, C. Das, C. Narayana, K.S. Rangappa, T.K. Kundu, Activation of p300 histone acetyltransferase by small molecules altering enzyme structure: probed by surface-enhanced Raman spectroscopy, J. Phys. Chem. B 111 (2007) 4527–4534.

[32] K. Balasubramanyam, R.A. Varier, M. Altaf, V. Swaminathan, N.B. Siddappa, U. Ranga, T.K. Kundu, Curcumin a novel p300/CREB-binding protein-specific inhibitor of acetyltransferase, represses the acetylation of histone/nonhistone proteins and histone acetyltransferase-dependent chromatin transcription, J. Biol. Chem. 279 (2004) 51163–51171.

[33] B. Devipriya, A. Renuga Parameswari, G. Rajalakshmi, T. Palvannan, P. Kumaradhas, P. Exploring the Binding affinities of p300 enzyme activators CTPB and CTB using docking method, Indian J. Biochem. Biophys. 47 (2010) 364–369.

[34] P. Munshi, T.N. Guru Row, Electron density study of 2*H*-chromene-2-thione, Acta Crystallogr. B 58 (2002) 1011–1017.

[35] P. Srinivasan, A. David Stephen, P. Kumaradhas, Effect of gold atom contact in conjugated system of one dimensional octane dithiolate based molecular wire: a theoretical charge density study, J. Mol. Struct: Theochem. 910 (2009) 112–121.

[36] A. David Stephen, M. Revathi, S.N. Asthana, Rajesh B. Pawar, P. Kumaradhas, Probing the weakest bond and the cleavage of p-chlorobenzaldehyde diperoxide energetic molecule via quantum chemical calculations and theoretical charge density analysis, Int. J. Quant. Chem. 111 (2011) 3741–3754.

[37] D.E. Hibbs, J.R. Hanrahan, M.B. Hursthouse, D.W. Knight, J. Overgaard, P. Turner, R.O. Piltz, M.P. Waller, Experimental and theoretical charge distribution in (*Z*)-*N*-methyl-*C*-phenylnitrone, Org. Biomol. Chem. 1 (2003) 1034–1040.

[38] E.J. Yearley, E.A. Zhurova, V.V. Zhurov, A. Alan Pinkerton, Binding of genistein to the estrogen receptor based on an experimental electron density study, J. Am. Chem. Soc. 129 (2007) 15013–15021.

[39] P.L.A. Popelier, Atom in Molecules an Introduction, Pearson Edition, Harlow, UK, 1999.

[40] G.U. Kulkarni, P. Kumaradhas, C.N.R. Rao, Charge density study of the polymorphs of *p*-nitrophenol, Chem. Mater. 10 (1998) 3498–3505.

[41] R.S. Mulliken, Electronic population analysis on LCAO-MO molecular wave functions, J. Chem. Phys. 23 (1955) 1833–1841.

[42] A.E. Reed, R.B. Weinstock, F.A. Weinhold, Natural population analysis, J. Chem. Phys. 83 (1985) 735–747.

[43] P. Coppens, Y. Abramov, M. Carducci, B. Korjov, I. Novozhilova, C. Alhambra, M.R. Pressprich, Experimental charge densities and intermolecular interactions: electrostatic and topological analysis of dl-histidine, J. Am. Chem. Soc. 121 (1999) 2585–2593.

[44] P. Politzer, J.S. Murray, Z. Peralta-inga, Molecular surface electrostatic potentials in relation to noncovalent interactions in biological systems, Int. J. Quant. Chem. 85 (2001) 676–684.